Processing and properties of PLA/Mg filaments for 3D printing of scaffolds for biomedical applications

C. Pascual-González[1], C. Thompson[1,2], J. de la Vega[1], N. Biurrun[1,3], J. P. Fernández-Blázquez[1], I. Lizarralde[1,3,4], D. Herráez-Molinero[1,3], C. González[1,3], J. LLorca[1,3,*]

[1] *IMDEA Materials Institute, C/Eric Kandel 2, 28906 -Getafe, Madrid, Spain.*
[2] *Department of Material Science and Engineering, Universidad Carlos III de Madrid, 28911 - Leganés, Madrid, Spain.*
[3] *Department of Materials Science, Polytechnic University of Madrid, E. T. S. de Ingenieros de Caminos, 28040 - Madrid, Spain.*
[4] *Hexcel Composites S.L., C/ Bruselas 10-16, 28983, Parla, Madrid, Spain.*

Abstract

Design and Methodology The mixture of poly-lactic acid pellets and Mg particles was extruded twice, the second time using a precision extruder that produces a filament with zero porosity, constant diameter and homogeneous dispersion of Mg particles. The physico-chemical properties of the extruded filaments were carefully analysed to determine the influence of Mg particles on the depolymerisation of poly-lactic acid during high temperature extrusion and the optimum melt flow index to ensure printability.

Purpose A novel strategy has been developed to manufacture poly-lactic acid filaments reinforced with Mg particles for fused filament fabrication of porous scaffolds for biomedical applications.

Findings It was found that the addition of a polyethylene glycol plasticizer was necessary to allow printing when the weight fraction of Mg was above 4%. It was possible to print porous face-center cubic scaffolds with good geometrical accuracy and minimum porosity with composite filaments containing polyethylene glycol.

*Corresponding author: javier.llorca@upm.es , javier.llorca@imdea.org

Originality/value The new strategy is easily scalable and seems to be very promising to manufacture biodegradable thermoplastic/metal composite filaments for 3D printing that can take advantage of the different properties of both components from the viewpoint of tissue engineering.

Keywords: Poly-lactic acid, Magnesium, Composites, Fused filament fabrication, Tissue engineering

---

1. Introduction

Biodegradable materials have received increasing attention in recent years for tissue engineering applications because a second surgery is not necessary to remove the implant after healing (Temenoff and Mikos, 2000; Sheikh et al., 2015; Godavitarne et al., 2017). Poly(lactic acid) (PLA) is a biocompatible and bioabsorbable polymer (da Silva et al., 2018) that has been used for wound dressing, tissue fixation, craniomaxillofacial surgery and bone fractures (Maurus and Kaeding, 2004). Nevertheless, PLA exhibits very long degradation times and limited mechanical properties for orthopaedic applications. Additionally, the accumulation of acidic products during degradation does not always favour tissue integration (Rokkanen et al., 2000). The incorporation of biodegradable Mg particles, which present much higher stiffness and much lower degradation time than PLA (Zhao et al., 2017b; Li et al., 2021), is an interesting strategy to optimize the properties for specific applications. Indeed, the acidic products generated during the degradation of PLA can be neutralized by the degradation of Mg particles (Zhao et al., 2017a). Moreover, PLA/Mg composites with better mechanical properties (creep strength and compression modulus) than the corresponding PLA have been manufactured (Cifuentes et al., 2016, 2017a; Brown et al., 2015).

PLA is also one of the most popular thermoplastic polymers for 3D printing through fused filament fabrication (FFF) (Tyler et al., 2016). This technique allows the fabrication of patient-specific scaffolds and implants from computer-assisted tomography medical images in orthopaedics and traumatology (Auricchio and Marconi, 2016). The production of PLA filaments reinforced with metallic particles for 3D printing is carried out through the extrusion of pellets of PLA/Mg which were produced by conventional extrusion (Antoniac et al., 2019) or by means of colloidal routes (Ferrández-Montero et al., 2019, 2020) that allow much higher volume fraction of Mg particles.

Nevertheless, these filaments are not optimal for 3D printing because of several issues. They include the inhomogeneous distribution of metallic particles within the filament (which also leads to porosity) (Díaz-García et al., 2020) and variations in the diameter of the filaments, which have been observed to impede continuous printing when the filament is fed into the extrusion nozzle of a FFF printer. Moreover, it is critical to control the rheological properties of the filaments which should be kept within the appropriate range for a given printing temperature (Waheed et al., 2019). It is known that MgO catalyzes the thermal degradation of PLA at the extrusion and printing temperatures (Feliu Jr et al., 2009; Esmaily et al., 2017; Motoyama et al., 2007), reducing the molecular weight (MW), viscosity and mechanical properties of the PLA/Mg composites (Cifuentes et al., 2017b).

In this investigation, a novel technique is presented to manufacture by extrusion PLA/Mg filaments with constant diameter, no porosity, homogeneous Mg particle distribution and controlled viscosity with or without the addition of a plasticizer. Moreover, the influence of the Mg particles on the depolymerisation of PLA during filament fabrication is ascertained by means of various physico-chemical characterization techniques to establish the optimum processing route towards 3D printing of scaffolds. Finally, porous PLA/Mg scaffolds were manufactured by FFF and their quality from the viewpoint of geometrical accuracy and mechanical properties was determined.

2. Methods

2.1. Filament fabrication

Ingeo Biopolymer 2003D from NatureWorks (NatureWorks BV) was selected as the PLA polymer matrix because it was used previously for 3D printing using the FFF technique (Cifuentes et al., 2016; Ferrández-Montero et al., 2019; Kovalcik et al., 2020; Cesur et al., 2019). In addition, polyethylene glycol (PEG) of low molecular weight (MW = 1000 g/mol) was selected as a plasticizer since it is one of the most common and effective agents (Farah et al., 2016). Spherical particles of WE43 Mg alloy were supplied by Meotec GmbH with a nominal composition of 1.4 - 4.2% Y, 2.5 - 3.5 % Nd, <1% (Al, Fe, Cu, Ni, Mn, Zn, Zr) and balance Mg (in wt.%). They were manufactured for selective laser melting applications and the powder particle distribution

was D10 = 29.1 μm, D50 = 45.8 μm and D90 = 64.4 μm (Li et al., 2021). The particles were covered with a thin passivation layer of Y_2O_3 which also limited the flammability of the powder during handling. Alloys with similar composition have been successfully applied in orthopaedics applications (Windhagen et al., 2013) and are well-established as biodegradable and biocompatible alloys (Zhao et al., 2017a).

The whole manufacturing process, starting from the PLA and Mg powders to the fabrication of scaffolds by FFF is shown in Fig. 1. First, PLA pellets were dried in a conventional oven at 60°C for 24 hours. Afterwards, they were manually mixed with Mg powder in the required weight proportions and it was ensured that most of the metallic particles remained adhered to the pellet surface. The mixture of PLA and Mg particles was extruded in a Xplore MC 15 Micro Compounder containing two conical mixing screws at 180°C with a residence time of $\sim$ 3 minutes and a screw rotating speed of 100 rpm (Fig. 1a). The extruded material went through an air-cooling channel attached to the extruder leading to a filament of $\approx$ 2.85 mm in diameter. It should be noted that the diameter of the filament could not be controlled in this step. The filaments were pelletized (Granulator, Brabender) and the corresponding feedstock of PLA/Mg pellets was introduced in a filament maker machine (Precision 450, 3Devo) (Fig. 1b). The 3Devo incorporates four independent controllable heaters along the mixing screw and the heater temperatures are indicated in Table 1 for each material. The heater temperatures were reduced with increasing Mg content because of the lower viscosity of the molten mixture, but the same temperature difference was maintained between consecutive heaters in the case of PLA/Mg composites. The residence time was $\sim$ 12 minutes. Addition of 5 wt. % of PEG to the composites with 4% and 5% Mg allowed to extrude the filaments at lower temperatures. The addition of 5% PEG was selected based on the literature, which reported improvements on the PLA processing and printability without compromising mechanical properties of the 3D printed scaffolds (Serra et al., 2014). The 3Devo filament maker includes a feedback control of the spooling system (based on optical sensor that measures *in situ* the filament diameter) to ensure that the filament diameter is constant after extrusion. The nominal diameter was set at 2.85 mm, which is the standard diameter supported by the Ultimaker S5 3D printer. The filaments were spooled and scaffolds were manufactured by FFF using a Ultimaker S5 printer (Fig. 1(c)).

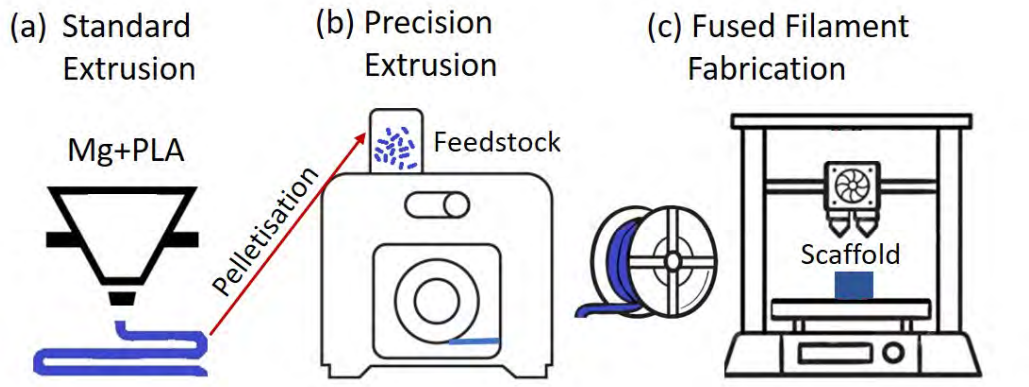

Figure 1: Schematic of the manufacturing process from the PLA and Mg powders to the fabrication of scaffolds by FFF. (a) Thermal mixing of raw materials (PLA and Mg powders) at 180°C, followed by extrusion. (b) Pellets of the extruded filaments were extruded again in a filament maker machine. (c) Extruded filaments were spooled and scaffolds were manufactured by FFF.

Material	heater 1	heater 2	heater 3	heater 4
PLA	180	200	180	170
PLA/Mg (1%, 2%, 3%)	170	190	170	160
PLA/Mg (4%, 5%)	160	180	160	150
PLA/Mg (4%, 5%)/PEG (5%)	150	160	150	140

Table 1: Temperature (in °C) of the successive heaters during precision extrusion of PLA/Mg composites. Mg and PEG content are expressed in wt. %.

2.2. Filament characterisation

The physical and chemical properties of the filaments were characterized after standard extrusion (in the Xplore MC 15 Micro Compounder) and precision extrusion (in the 3Devo extruder). The Mg particle distribution in addition to the porosity were measured in filaments of 3 mm in length by means of X-ray computed micro-tomography (X-μCT) in a Phoenix Nanotom using a W target and 0-mode nanofocus. The voltage of the X-ray tube was set to 80 kV and the current was 150 μA and the voxel size in the tomograms was 2 μm.

The thermal characterisation of PLA/Mg composite filaments was performed by differential scanning calorimetry (DSC) (Q200, TA Instruments) up to 180°C with a heating/cooling rate of 10°C/min. Thermal degradation of PLA/Mg specimens up to 500°C in air was studied by thermo-gravimetric analysis (TGA) (Q50, TA Instruments) which provided the weight variation as a function of the temperature. The MW distribution of the different PLA/Mg composites was measured by gel permeation chromatography (GPC) (GPC 2414, Waters) including a Waters 2424 refractive index detector and a series of narrow polystyrene standards with Tetrahydrofuran as the mobile phase.

Melt flow index (MFI) tests of standard and precision extruded filaments were performed by using a MFI tester (KJ-3092, Kinsgeo) with a load of 2,16 Kg for 10 minutes at 170°C and 190°C following ASTM standard D1238. Finally, the mechanical properties of the filaments in tension were measured in an electro-mechanical mechanical testing machine (Instron 3384) under displacement control at displacement rate of 0.5 mm/min. Load was determined using a load cell and deformation with an extensometer of 12.5 mm gage length attached to the filament.

2.3. Specimen fabrication and mechanical characterisation

An Ultimaker S5 was used to print the PLA/Mg specimens using the precision extruded filaments, with a travel speed of 5 mm/s and a nozzle of 400 μm in diameter. The printing temperature varied in the range 170°C to 210°C depending on the PLA/Mg filament composition while the bed temperature was kept at 60°C. Dog-bone specimens with a rectangular cross section of 5 x 2 mm^2, following ISO 527-1 type 1BA (Iso, 2012; Martínez et al., 2012; Butt et al., 2019), were printed to measure the mechanical properties in tension.

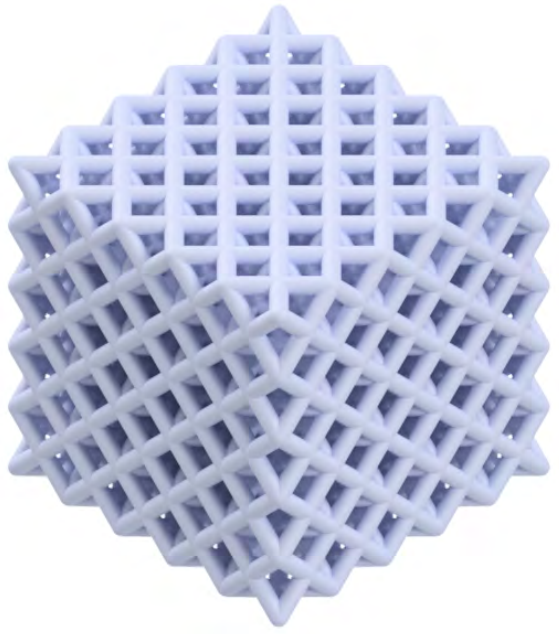

Figure 2: Model of the fcc scaffold.

Tensile tests were carried out in an electromechanical mechanical testing machine (Instron 3384) and deformation was measured with an extensometer of 12.5 mm gage length attached to the sample. In addition, porous scaffolds with a face-centered cubic (fcc) lattice were printed. The dimensions of the scaffolds were of 20 x 20 x 20 mm^3 and they were made up by circular struts of 1.5 mm in diameter (Fig. 2). The microstructure of selected scaffolds was analyzed by means of X-μCT with the same voltage and current used in the case of the filaments but different sample and detector positioning, leading to a voxel size of 12 μm. In addition, the mechanical properties of the scaffolds in compression were measured using Instron 3384 mechanical testing machine. The cubic scaffolds were compressed between two compression plates under displacement control at cross-head speed of 0.5 mm/min. Teflon paste was inserted between the scaffold and the compression plates to minimize friction. The applied load was measured with a load cell while the reduction in length was determined by means of a linear variable differential transducer in contact with the compression plates.

Mg content (wt. %)	Standard extrusion	Precision extrusion
1%	0.45	0
2%	2.72	0
3%	4.91	0
4%	0.61	0.03
5%	0.84	0

Table 2: Pore volume fraction (in %) in PLA/Mg filaments processed by standard and precision extrusion.

3. Results and discussion

3.1. Geometrical features of filaments

Filaments with different weight fractions of Mg (x= 1%, 2%, 3%, 4% and 5%) and a target diameter of 2.85 mm were manufactured by standard and precision extrusion. Representative sections of the filament microstructure obtained by X-μCT are depicted in Figs. 3a and b, respectively, for standard and precision extruded filaments. Black regions stand for pores while white regions are the spherical Mg particles. Spherical pores of88 ± 19 μm in diameter were found in the filaments produced by standard extrusion regardless of the Mg content. The pore volume fraction was measured by segmentation of the tomograms in filaments of 3 mm in length and can be found in Table 2. Large pores were found in the filaments after standard extrusion and, in addition, the filaments presented large variations in diameter and shape along their length. These features hinder their use during FFF, as the printing process is often stopped as a result of the pores and of the variations in the filament diameter.

On the contrary, precision extrusion led to filaments with 0 or negligible porosity (Fig. 3b and Table 2). Moreover, the filament diameter was successfully controlled during precision extrusion (Fig. 4), as shown by the *in situ* measurements of the filament diameter during extrusion of a PLA/5% Mg composite, which was the most difficult filament to produce. Oscillations in the diameter between 2.92 mm and 2.76 mm were observed while the average diameter was 2.850 ± 0.004 mm. The fluctuations of 3% in the diameter did not impede the continuous printing by the FFF method. All of the PLA/Mg composite filaments manufactured by precision extrusion were

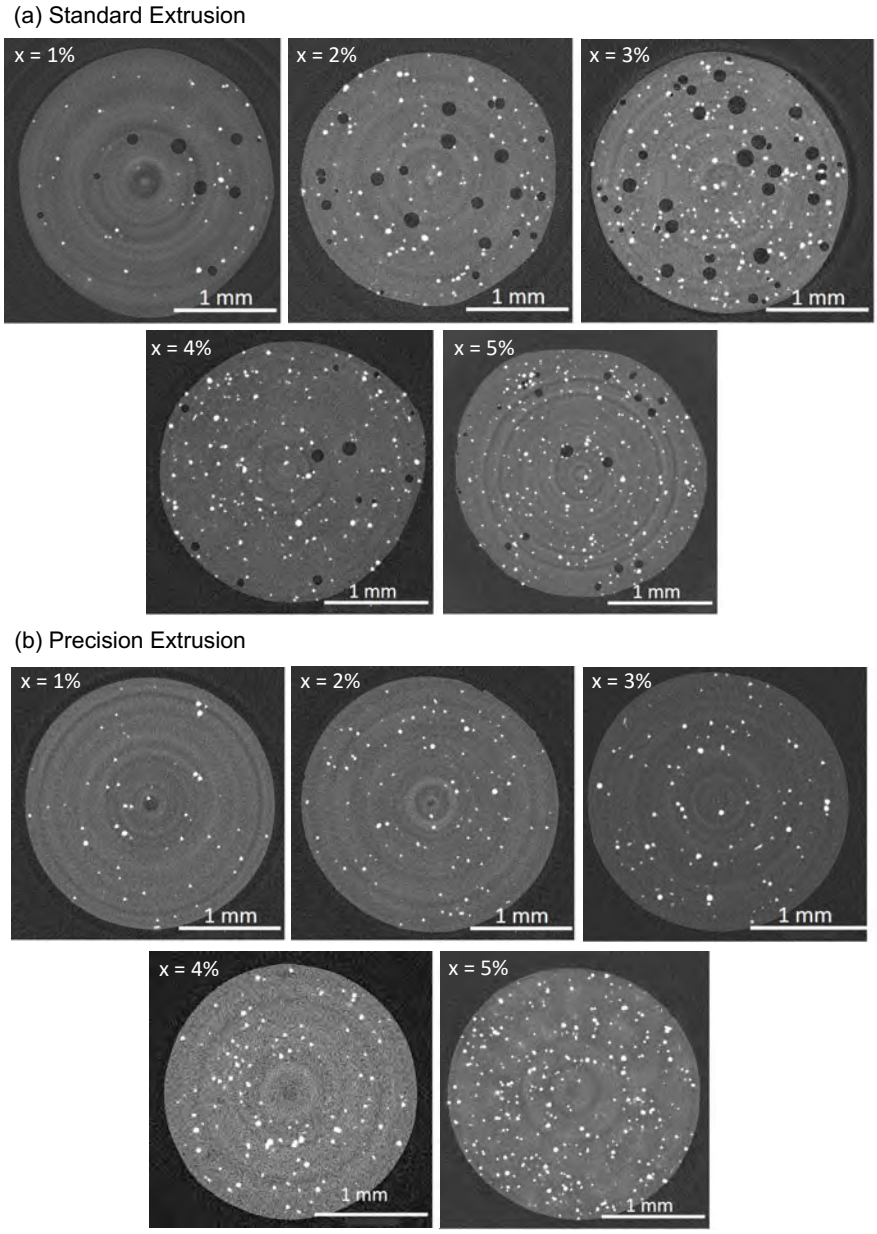

Figure 3: Representative cross sections obtained by X-μCT of PLA/Mg filaments after (a) standard extrusion and (b) precision extrusion. x stands for the weight fraction of Mg. Filament diameter was 2.85 mm in all cases.

within this tolerance in terms of diameter and could be successfully used to print scaffolds with complex geometries. Moreover, precision extrusion was a reproducible and robust process, demonstrating its potential for large scale production of composite filaments.

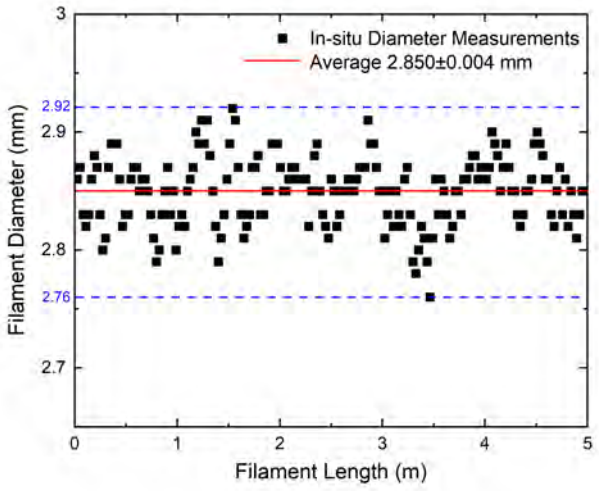

Figure 4: Oscillations of the filament diameter along the filament during precision extrusion of a PLA/5% Mg composite.

3.2. Physico-chemical properties of filaments

Filament extrusion involves melting and shearing and these processes may modify the structure and MW of the polymer. Thus, the physico-chemical properties of the filaments after standard and precision extrusion were carefully analyzed by DSC, TGA and GPC to determine the impact of processing on the PLA properties.

The heat flow curves of PLA/Mg composites for the first heating after standard and precision extrusion are plotted in Figures 5a and 5b, respectively. The same curves for the PLA/4% Mg and PLA/5% Mg composites with 5% PEG after precision extrusion are plotted in Figure 5c. Three thermal transitions are observed in all samples, independently of the Mg concentration or the presence of PEG. The first transition with increasing temperature is an endothermic step associated with the glass transition of PLA (T_g). All of the PLA/Mg samples presented this transition at 58°C, even after the

two extrusion processes. This fact indicates that Mg has no plasticizer effect and that PLA depolymerization after extrusion was not large enough to increase the local chain mobility. It should be noted that the T_g for pure PLA after standard extrusion is around 58-60 °C and after precision extrusion is approximately 2°C higher. This small shift could be explained by the ageing of the PLA samples during storage. The sample densifies at room temperature after some time, decreasing the chain mobility and slightly increasing the T_g. On the other hand, the addition of low molecular weight PEG had a clear and expected plasticizer effect (Yeh et al., 2009; Baiardo et al., 2003) reducing the T_g to $\sim$ 51°C (Figure 5c). An exothermic process due to cold crystallization (T_{cc}) appeared in all samples at higher temperature. The presence of Mg shifted the exothermic peak from 122°C in neat PLA to 116°C in PLA/5% Mg after standard extrusion, and a similar reduction has been reported in the literature (Antoniac et al., 2019). This behavior may be produced by two mechanisms, namely the nucleating effect of Mg particles and the higher polymer chain mobility due to the lower MW of PLA after depolymerization during extrusion, as discussed below. T_{cc} further decreased to 111°C in PLA/5% Mg after precision extrusion and the differences after standard and precision extrusion can be explained by the higher reduction in MW due to the PLA depolymerization during precision extrusion as well as by the increase of the polymer chain mobility due to the reduction of the physical entanglements during the extrusion process. The increase of chain mobility is much more important in the presence of PEG plasticizer, leading to the lowest T_{cc} (Figure 5c) (Requena et al., 2016). Finally, PLA presented a melting peak (T_m) at 150°C, which remained constant for all the standard extruded composites and for the precision extruded composites up to 3% Mg. Nevertheless, the shape of the peak became broader with increasing Mg content and T_m decreased slightly in the precision extruded composites with 4% and 5% Mg, while a new endothermic peak appeared at higher temperature. This behavior can be explained by the relation between T_{cc} and T_m. Crystallization at lower temperature produced less perfect crystals which melt at lower temperature, and that can recrystallize at slightly higher temperature. This melt-recrystallization-melt process was more evident in the samples containing PEG, which presented the lowest T_{cc} and where both melting peaks were clearly observed (Figure 5c).

The weight loss as a function of temperature obtained from TGA is plotted in Figure 6 for the precision extruded composites with different weight

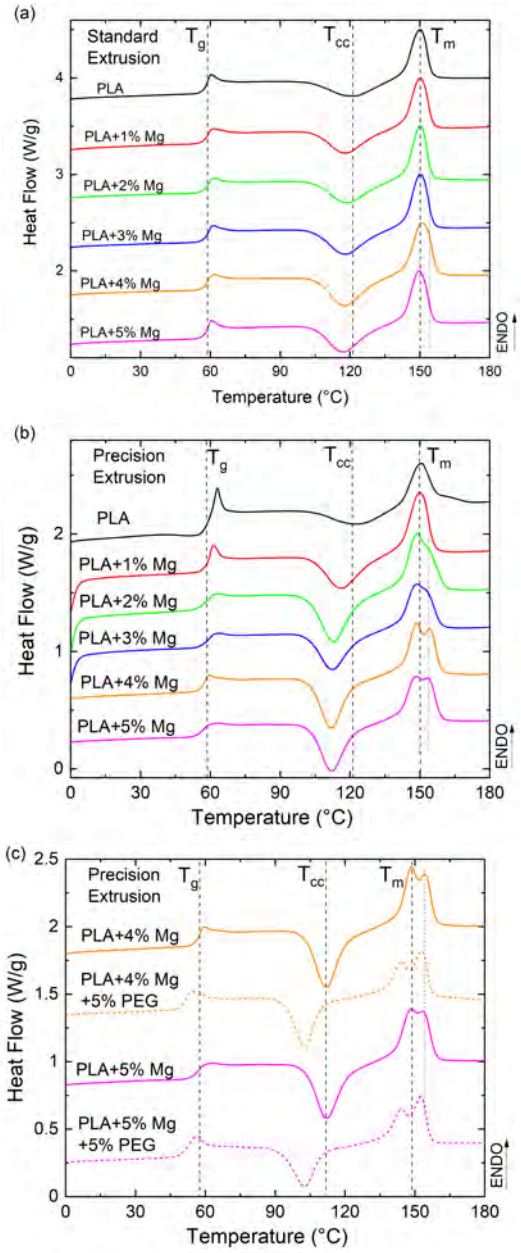

Figure 5: Heat flow curves of PLA/Mg filaments during DSC at a heating rate of 10°C/min. (a) After standard extrusion. (b) After precision extrusion. (c) Effect of PEG on the heat flow of PLA/Mg filaments. Glass transition temperature (T_g), cold crystallization termperature (T_{cc}), and melting point (T_m) are indicated with dashed lines.

fractions of Mg particles. All samples undergo one simple thermal decomposition step. Pure PLA degradation started at $\sim$ 300°C and reached the maximum weight loss at $\sim$ 371°C. The onset degradation temperature decreased as the Mg content increased. Thermal degradation started at $\sim$ 217°C and the maximum weight loss was reached at $\sim$ 298°C when the Mg weight fraction was 5%. This trend has been previously reported for PLA/Mg composites because PLA is degraded by depolymerization in the presence of Mg particles (Cifuentes et al., 2017b) and the reduction in MW may trigger degradation at lower temperatures (Carrasco et al., 2010). It should be noted, however, that the onset degradation temperatures were always higher than the processing temperatures during extrusion and printing but the progressive reduction of the degradation temperature with higher Mg loads may become a problem to print filaments with higher Mg content (Lim et al., 2008).

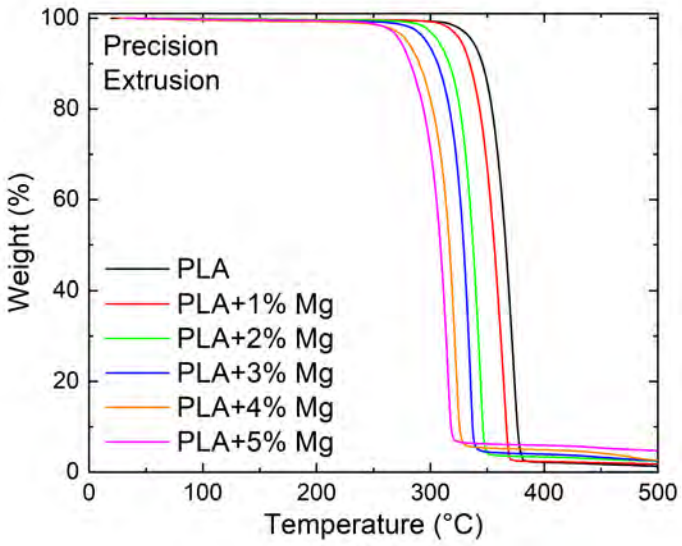

Figure 6: Weight loss as a function of temperature obtained from TGA for the precision extruded composite containing different weight fractions of Mg particles.

The MW distributions (MWD) of PLA and PLA/Mg composites with 3, 4 and 5% of Mg obtained by GPC are plotted in Figs. 7a and b after standard and precision extrusion, respectively. Standard extrusion was carried out at 180°C and the MW distribution of extruded PLA was very similar to the one measured in the as-received PLA pellets (not shown in the figure), indicating

that extrusion at this temperature did not reduce the MW. Moreover, the MW was independent of the Mg content in the PLA/Mg composites obtained by standard extrusion, except for the one with 5% Mg that showed a shift towards lower MWs. However, a large shift towards lower MWs was found in all the PLA/Mg composites after precision extrusion and the reduction was particularly important in the composite with 5% Mg. These results are summarized in Fig. 7d, where the average number MW, Mn, after standard and precision extrusion is plotted as a function of the Mg content. They show that neat PLA degradation is limited during standard extrusion (maximum temperature 180°C, residence time 3 minutes) and more noticeable after precision extrusion (maximum temperature 200°C, residence time 12 minutes). The same trend was observed in the composites with Mg although the reduction in MW was much more important. The maximum temperatures during precision extrusion of PLA/Mg filaments were either 190°C or 180°C (Table 1), very similar to the maximum temperature during standard extrusion (180°C). However, the residence time during precision extrusion was much longer (12 minutes as compared with 3 minutes for standard extrusion) and the overall reduction in the MW was higher during precision extrusion due to the catalytic effect of the Mg particles on the PLA depolymerisation.

Large reductions in the MW of PLA lead to large decreases in viscosity and compromise the mechanical properties. Thus, 5 wt. % of PEG was added to the PLA/Mg mixture with 4% and 5% Mg to reduce the processing temperature during precision extrusion. In this case, the maximum temperature for precision extrusion was 160°C (Table 1) and, as result, the shift towards lower MW distributions was reduced in comparison with the composites extruded without PEG (Fig. 7c). The shoulder at low MW of filaments with PEG was attributed to the presence of low MW PEG. Overall, the TGA profile of PLA in the precision extruded filaments with PEG was similar to the degradation of the standard extruded filaments without PEG (Fig. 7d).

MFI tests were performed in the standard extruded and precision extruded filaments to assess the the printability of the filaments as well as to determine the optimum printing temperature. According to the literature, the MFI of the filament should be in the range of 10 g/10 min to 30 g/10 min to be successfully printed by the FFF technique (Wang et al., 2018). The appropriate viscosity is necessary to ensure that the molten material flows easily through the nozzle but the viscosity has to be high enough to support the weight of the printed layers. The evolution of the MFI at 190°C with the

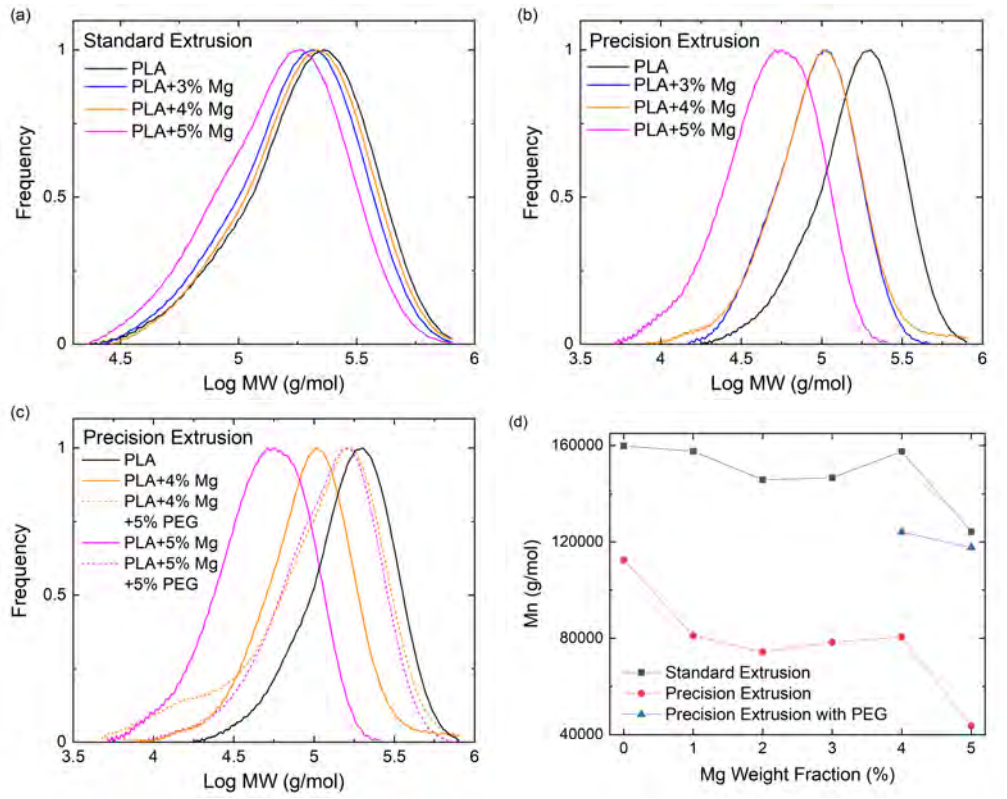

Figure 7: Molecular weight distributions of PLA/Mg composites. (a) After standard extrusion. (b) After precision extrusion. (c) Effect of PEG on the molecular weight distribution after precision extrusion. (d) Evolution of the average molecular weight with Mg content after standard and precision extrusion.

Mg content for standard and precision extruded filaments is plotted in Figure 8a. The MFI increased with the Mg content and the differences between both types of filaments were small when the Mg content was $\leq 2\%$. The MFI was close to the lower printability limit. However, large differences between both types of filaments were found for higher Mg contents. The MFI of standard extruded filaments increased with Mg content (except for the highest Mg loads of 5%) but it was always within the printability range. Nevertheless, the MFI of precision extruded filaments with 3% and 4% of Mg was very high and outside of the printability limit. The low viscosity of these filaments can be attributed to the reduction of the PLA MW during precision extrusion (Figure 7d). Surprisingly, the MFI of the precision extruded filament with

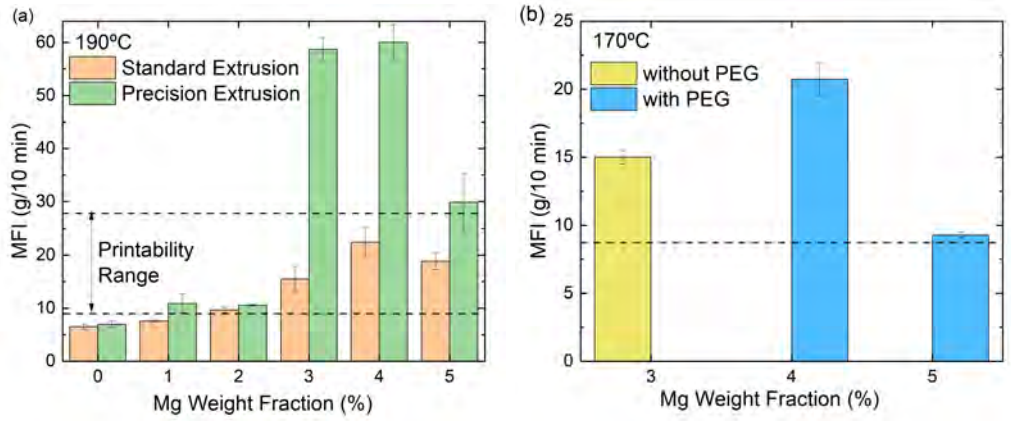

Figure 8: (a) MFI at 190°C of standard extruded and precision extruded PLA/Mg filaments as a function of the Mg content. (b) MFI at 170°C of precision extruded filaments of PLA/Mg and PLA/Mg/5%PEG as a function of the Mg content. The MFI range for printability is marked by the horizontal dashed lines.

5% Mg was lower than that of the filaments with 3% and 4% of Mg and this behavior could be attributed to the increase in viscosity associated with the larger volume fraction of Mg particles in the molten polymer. Thus, filaments produced by standard extrusion showed MFI within the printability range but they could not be used because of the porosity and inhomogeneities in the diameter. The viscosity of precision extruded filaments of pure PLA and of PLA with Mg content up to 3% was also within the printability range at 190°C and they were successfully used for 3D printing of scaffolds. However, 3D printing of PLA-3% Mg, PLA-4% Mg and PLA-5% Mg failed, even if the latter was within the printability range.

The MFI at 170°C of precision extruded PLA-3% Mg was within the printability range and it could be printed at this temperature (Figure 8b). Nevertheless, it was not possible to determine the MFI of precision extruded PLA-4% Mg at 170°C due to clogging in the nozzle. 3D printing of this material was possible, although it was complicated and required user intervention several times. To overcome these problems, precision extrusion of filaments of PLA-4% Mg- 5% PEG and PLA-5% Mg- 5% PEG were processed at the temperatures indicated in Table 1. The MFI at 170°C of the precision extruded filaments with PEG are shown in Figure 8b and both were within the printability range. Moreover, they were successfully printed at this temperature.

3.3. Mechanical properties of dog-bone specimens

The tensile stress-strain curves measured in dog-bone specimens of PLA, PLA-4% Mg and PLA-4% Mg with 5% PEG are shown in Figure 9. The specimens were printed with a raster angle of 0° (parallel to the loading direction) and a layer thickness of 0.1 mm. The elastic moduli of the three materials was very similar (around 3 GPa) but the tensile strength of PLA and PLA-4% Mg was higher (around 45 MPa) than that of PLA-4% Mg with 5% PEG (33 ± 1 MPa). Overall, these mechanical properties are comparable to those reported for PLA for biomedical applications (Farah et al., 2016) and the reduced strength of the composites with PEG can be attributed to the increase in the polymer chains mobility induced by the presence of PEG.

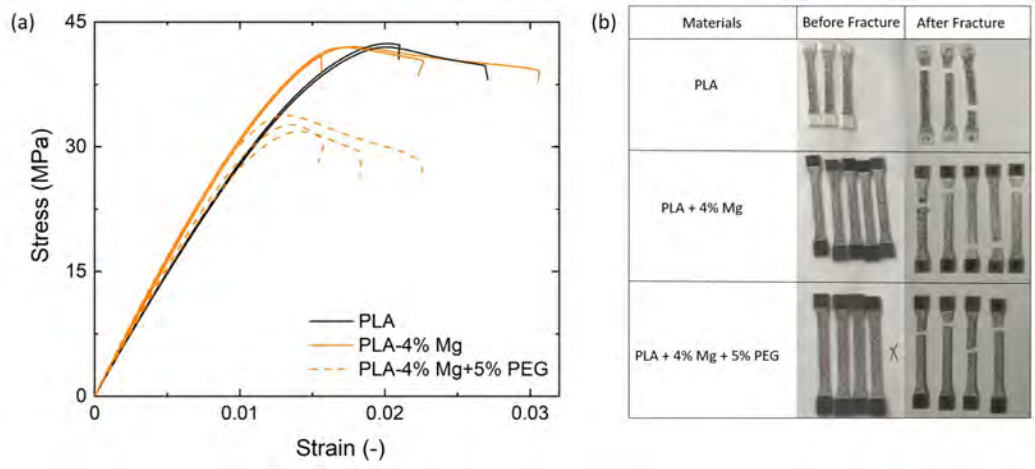

Figure 9: (a) Tensile stress-strain curves of dog-bone specimens of pure PLA, PLA-4% Mg and PLA-4% Mg with 5% PEG deformed parallel to the printing direction. (b) Images of the specimens after fracture.

3.4. Structure and mechanical properties of porous scaffolds

Porous scaffolds based on a fcc lattice (Fig. 2) were manufactured with precision extruded filaments of PLA, PLA/4% Mg and PLA/4% Mg/5% PEG in an Ultimaker S5 FFF printer. No special modifications were required to print the porous structures besides a slight increase of the tension on the feeder and a slow printing speed of 5 mm/s. The printing temperatures were selected based on the MFI experiments (Fig. 8) and they were 210°C for neat PLA and 170°C for PLA /4% Mg and PLA/4% Mg/5% PEG. The

Table 3: Mechanical properties of the 3D printed dogbone specimens tested in tension and of the FCC scaffolds deformed in compression.

	Tensile dogbone specimens			Scaffold in compression	
Material	Elastic Modulus (GPa)	Strength (MPa)	Strain at break (%)	Elastic Modulus (MPa)	Strength (MPa)
PLA	3.1±0.2	45±5	2.1±0.4	650±32	16±1
PLA-4% Mg	3.1±0.1	42±1	2.3±0.8	540±48	15±1
PLA-4% Mg+5%PEG	3.0±0.2	33±1	2.2±0.3	533±18	13±1

microstructure of the scaffolds was analyzed by means of X-μCT to assess the geometric accuracy and the internal porosity. Representative tomograms of the scaffolds printed with the three filaments are shown in Figure 10. They show that it was possible to print the scaffolds with the complex fcc shape with good geometrical accuracy with the three filaments. However, large internal porosity was found in the PLA/4%Mg scaffolds (Fig. 10b) as compared with those printed with pure PLA filaments (Fig. 10a). The addition of PEG to the filaments reduced the internal porosity of the scaffolds while it was possible to print the scaffolds at lower temperatures.

The engineering stress-strain curves of the fcc scaffolds in compression are plotted in Fig. 11. They were calculated from the applied load and displacement taking into account the initial height and cross-section of the scaffolds. The videos of the mechanical tests of the fcc scaffolds of PLA/4% Mg and PLA/4% Mg/5% PEG can be found in the videos of the Supplementary Material. All the scaffolds showed a ductile behavior during deformation and the initial elastic region was followed by a plateau region in which the deformation progressed at constant stress. The videos in the supplementary material show that deformation was homogeneous during deformation leading to the adoption of a "barrel" shape for very large strains. The best mechanical properties were measured in the PLA scaffolds because of the low internal porosity (Fig. 10(a)) and of the higher strength of the material (Fig. 9). The elastic modulus and strength of the PLA/4% Mg and PLA/4% Mg/5% PEG scaffolds was reduced due to the porosity (Fig. 10(a)) or to the lower strength of the material (Fig. 9, respectively. The average values of the mechanical properties of the 3D printed dogbone specimens tested in tension and of the FCC scaffolds deformed in compression are summarised in Table 3. Nevertheless, it should be noticed that the differences were not very relevant and the addition of PEG facilitates the 3D printing of fully dense scaffolds at lower temperatures.

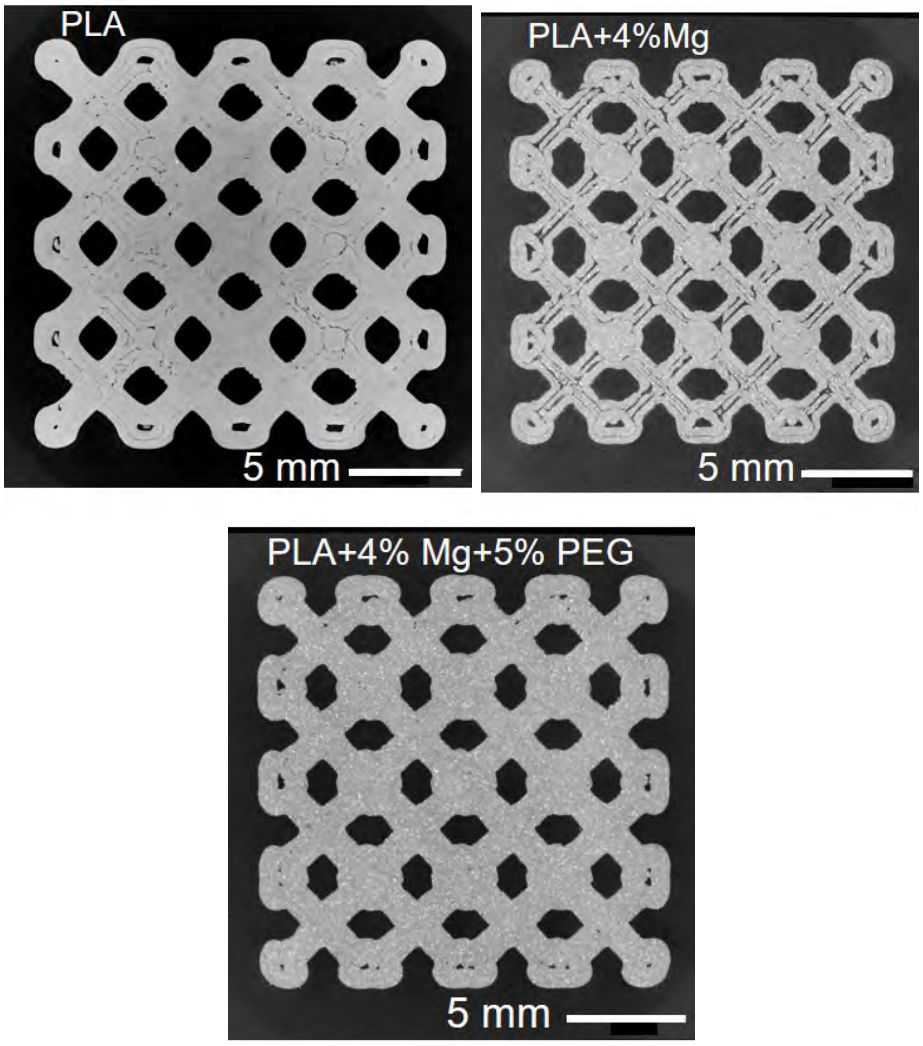

Figure 10: Cross-sections fcc scaffolds extracted from the tomograms obtained by X-μCT. (a) PLA. (b) PLA/4% Mg. (c) PLA/4% Mg/5% PEG.

4. Conclusions

A strategy has been developed to manufacture PLA filaments reinforced with Mg particles for the fused filament fabrication of porous scaffolds for biomedical applications. The mixture of PLA pellets and Mg particles was extruded twice, the second time using a precision extruder that allows the

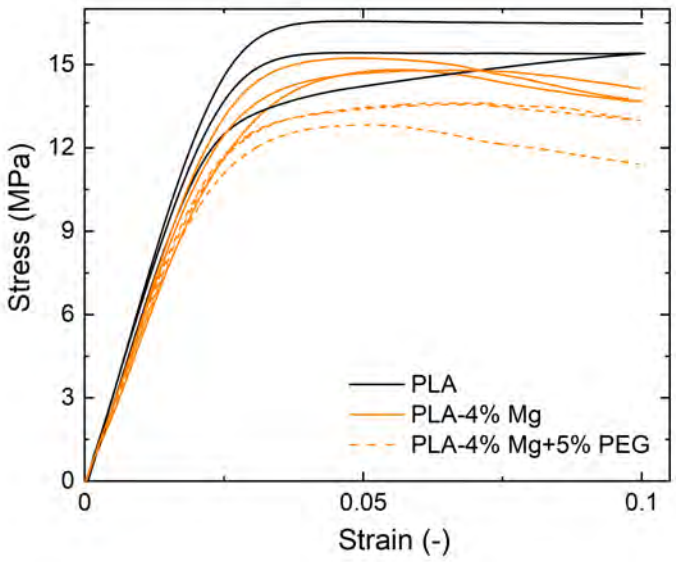

Figure 11: Experimental engineering stress-strain curves in compression of fcc scaffolds.

production of filaments with zero porosity, constant diameter and homogeneous dispersion of Mg particles. It was found that the long residence time ($>$ 10 minutes) at high temperatures (180-190°C) during precision extrusion led to a marked reduction in the molecular weight of PLA due to the thermal degradation of the polymeric chains catalyzed by the presence of the Mg particles. As a result, the flowability of the PLA/Mg composite was increased and therefore it was outside of the printability range when the weight fraction of Mg was $>$ 4%. The addition of PEG to the PLA/Mg composite reduced the precision extrusion temperature to 160°C and -consequently- the molecular weight of PLA was also reduced.

The tensile properties of solid specimens of PLA manufactured by fused filament fabrication were similar to those of standard PLA and the addition of Mg particles did not modify significantly the elastic modulus and the strength. However, addition of PEG reduced the strength due to enhanced chain mobility induced by the presence of the plasticizer. It was possible to print porous fcc scaffolds with good geometrical accuracy using PLA, PLA/4% Mg and PLA/4% Mg/5% PEG filaments with a commercial printer. The lowest internal porosity was achieved in scaffolds manufactured with PLA or PLA/4% Mg/5% PEG filaments and the best mechanical prop-

erties (elastic modulus and compressive strength) were achieved in the PLA scaffolds, although the properties of the PLA/4% Mg scaffolds were very similar. The scaffolds manufactured with PLA/4% Mg/5% PEG filaments could be printed at lower temperatures but the strength was reduced due to the effect of PEG in the polymer chain mobility. This manufacturing route -that can be easily scaled- seems to be very promising to manufacture biodegradable thermoplastic/metal composite filaments for 3D printing that can take advantage of the different properties of both components from the viewpoint of tissue engineering.

Acknowledgements

This investigation was supported by the European Unions Horizon 2020 research and innovation programme under the European Training Network BioImpant (Development of improved bioresorbable materials for orthopaedic and vascular implant applications), Marie Sklodowska-Curie grant agreement 813869. Additional support from the Spanish Ministry of Science and Innovation through the project ADDICOMP (grant RTI2018-094435-B-C33) is gratefully acknowledged.

References

Antoniac, I., Popescu, D., Zapciu, A., Antoniac, A., Miculescu, F., Moldovan, H., 2019. Magnesium filled polylactic acid (pla) material for filament based 3d printing. Materials 12 (5), 719.

Auricchio, F., Marconi, S., 2016. 3d printing: clinical applications in orthopaedics and traumatology. EFORT open reviews 1 (5), 121–127.

Baiardo, M., Frisoni, G., Scandola, M., Rimelen, M., Lips, D., Ruffieux, K., Wintermantel, E., 2003. Thermal and mechanical properties of plasticized poly (l-lactic acid). Journal of Applied Polymer Science 90 (7), 1731–1738.

Brown, A., Zaky, S., Ray Jr, H., Sfeir, C., 2015. Porous magnesium/plga composite scaffolds for enhanced bone regeneration following tooth extraction. Acta Biomaterialia 11, 543–553.

Butt, J., Hewavidana, Y., Mohaghegh, V., Sadeghi-Esfahlani, S., Shirvani, H., 2019. Hybrid manufacturing and experimental testing of glass fiber enhanced thermoplastic composites. Journal of Manufacturing and Materials Processing 3 (4), 96.

Carrasco, F., Pagès, P., Gámez-Pérez, J., Santana, O., Maspoch, M. L., 2010. Processing of poly (lactic acid): Characterization of chemical structure, thermal stability and mechanical properties. Polymer Degradation and Stability 95 (2), 116–125.

Cesur, S., Oktar, F. N., Ekren, N., Kilic, O., Alkaya, D. B., Seyhan, S. A., Ege, Z. R., Lin, C.-C., Kuruca, S. E., Erdemir, G., et al., 2019. Preparation and characterization of electrospun polylactic acid/sodium alginate/orange oyster shell composite nanofiber for biomedical application. Journal of the Australian Ceramic Society, 1–11.

Cifuentes, S. C., Frutos, E., Benavente, R., Lorenzo, V., González-Carrasco, J. L., 2017a. Assessment of mechanical behavior of pla composites reinforced with mg micro-particles through depth-sensing indentations analysis. Journal of the Mechanical Behavior of Biomedical Materials 65, 781–790.

Cifuentes, S. C., Gavilán, R., Lieblich, M., Benavente, R., González-Carrasco, J. L., 2016. In vitro degradation of biodegradable polylactic acid/magnesium composites: Relevance of mg particle shape. Acta Biomaterialia 32, 348–357.

Cifuentes, S. C., Lieblich, M., López, F., Benavente, R., González-Carrasco, J. L., 2017b. Effect of mg content on the thermal stability and mechanical behaviour of plla/mg composites processed by hot extrusion. Materials Science and Engineering: C 72, 18–25.

da Silva, D., Kaduri, M., Poley, M., Adir, O., Krinsky, N., Shainsky-Roitman, J., Schroeder, A., 2018. Biocompatibility, biodegradation and excretion of polylactic acid (pla) in medical implants and theranostic systems. Chemical Engineering Journal 340, 9–14.

Díaz-García, Á., Law, J., Cota, A., Bellido-Correa, A., Ramírez-Rico, J., Schäfer, R., Franco, V., 2020. Novel procedure for laboratory scale production of composite functional filaments for additive manufacturing. Materials Today Communications 24, 101049.

Esmaily, M., Svensson, J., Fajardo, S., Birbilis, N., Frankel, G., Virtanen, S., Arrabal, R., Thomas, S., Johansson, L., 2017. Fundamentals and advances in magnesium alloy corrosion. Progress in Materials Science 89, 92–193.

Farah, S., Anderson, D. G., Langer, R., 2016. Physical and mechanical properties of pla, and their functions in widespread applicationsa comprehensive review. Advanced drug delivery reviews 107, 367–392.

Feliu Jr, S., Pardo, A., Merino, M., Coy, A., Viejo, F., Arrabal, R., 2009. Correlation between the surface chemistry and the atmospheric corrosion of az31, az80 and az91d magnesium alloys. Applied Surface Science 255 (7), 4102–4108.

Ferrández-Montero, A., Lieblich, M., Benavente, R., González-Carrasco, J. L., Ferrari, B., 2020. Study of the matrix-filler interface in pla/mg composites manufactured by material extrusion using a colloidal feedstock. Additive Manufacturing 33, 101142.

Ferrández-Montero, A., Lieblich, M., González-Carrasco, J. L., Benavente, R., Lorenzo, V., Detsch, R., Boccaccini, A., Ferrari, B., 2019. Development of biocompatible and fully bioabsorbable pla/mg films for tissue regeneration applications. Acta biomaterialia 98, 114–124.

Godavitarne, C., Robertson, A., Peters, J., Rogers, B., 2017. Biodegradable materials. Orthopaedics and trauma 31 (5), 316–320.

Iso, E., 2012. 527-1. plasticsdetermination of tensile propertiespart 1: General principles. International Organization of Standardization: Geneva, Switzerland.

Kovalcik, A., Sangroniz, L., Kalina, M., Skopalova, K., Humpolíček, P., Omastova, M., Mundigler, N., Müller, A. J., 2020. Properties of scaffolds prepared by fused deposition modeling of poly (hydroxyalkanoates). International Journal of Biological Macromolecules 161, 364–376.

Li, M., Benn, F., Derra, T., Kroeger, N., Zinser, M., Smeets, R., Molina-Aldareguía, J. M., Kopp, A., LLorca, J., 2021. Microstructure, mechanical properties, corrosion resistance and cytocompatibility of WE43 Mg alloy scaffolds fabricated by laser powder bed fusion for biomedical applications. Materials Science and Engineering C 119, 111623.

Lim, L.-T., Auras, R., Rubino, M., 2008. Processing technologies for poly (lactic acid). Progress in Polymer Science 33 (8), 820–852.

Martínez, J., Diéguez, J., Ares, J., Pereira, A., Pérez, J., 2012. Modelization and structural analysis of fdm parts. In: AIP Conference Proceedings. Vol. 1431. American Institute of Physics, pp. 842–848.

Maurus, P. B., Kaeding, C. C., 2004. Bioabsorbable implant material review. Operative Techniques in Sports Medicine 12 (3), 158–160.

Motoyama, T., Tsukegi, T., Shirai, Y., Nishida, H., Endo, T., 2007. Effects of mgo catalyst on depolymerization of poly-l-lactic acid to l, l-lactide. Polymer degradation and stability 92 (7), 1350–1358.

Requena, R., Jiménez, A., Vargas, M., Chiralt, A., 2016. Effect of plasticizers on thermal and physical properties of compression-moulded poly [(3-hydroxybutyrate)-co-(3-hydroxyvalerate)] films. Polymer Testing 56, 45–53.

Rokkanen, P. U., Böstman, O., Hirvensalo, E., Mäkelä, E. A., Partio, E. K., Pätiälä, H., Vainionpää, S., Vihtonen, K., Törmälä, P., 2000. Bioabsorbable fixation in orthopaedic surgery and traumatology. Biomaterials 21 (24), 2607–2613.

Serra, T., Ortiz-Hernandez, M., Engel, E., Planell, J. A., Navarro, M., 2014. Relevance of PEG in PLA-based blends for tissue engineering 3D-printed scaffolds. Materials Science and Engineering: C 38, 55–62.

Sheikh, Z., Najeeb, S., Khurshid, Z., Verma, V., Rashid, H., Glogauer, M., 2015. Biodegradable materials for bone repair and tissue engineering applications. Materials 8 (9), 5744–5794.

Temenoff, J. S., Mikos, A. G., 2000. Injectable biodegradable materials for orthopedic tissue engineering. Biomaterials 21 (23), 2405–2412.

Tyler, B., Gullotti, D., Mangraviti, A., Utsuki, T., Brem, H., 2016. Polylactic acid (pla) controlled delivery carriers for biomedical applications. Advanced Drug Delivery Reviews 107, 163–175.

Waheed, S., Cabot, J. M., Smejkal, P., Farajikhah, S., Sayyar, S., Innis, P. C., Beirne, S., Barnsley, G., Lewis, T. W., Breadmore, M. C., et al.,

2019. Three-dimensional printing of abrasive, hard, and thermally conductive synthetic microdiamond–polymer composite using low-cost fused deposition modeling printer. ACS applied materials & interfaces 11 (4), 4353–4363.

Wang, S., Capoen, L., Dhooge, D. R., Cardon, L., 2018. Can the melt flow index be used to predict the success of fused deposition modelling of commercial poly (lactic acid) filaments into 3d printed materials? Plastics, Rubber and Composites 47 (1), 9–16.

Windhagen, H., Radtke, K., Weizbauer, A., Diekmann, J., Noll, Y., Kreimeyer, U., Schavan, R., Stukenborg-Colsman, C., Waizy, H., 2013. Biodegradable magnesium-based screw clinically equivalent to titanium screw in hallux valgus surgery: short term results of the first prospective, randomized, controlled clinical pilot study. BioMedical Engineering OnLine 12, 62.

Yeh, J.-T., Huang, C.-Y., Chai, W.-l., Chen, K.-N., 2009. Plasticized properties of poly (lactic acid) and triacetine blends. Journal of Applied Polymer Science 112 (5), 2757–2763.

Zhao, C., Wu, H., Ni, J., Zhang, S., Zhang, X., 2017a. Development of pla/mg composites for orthopedic implant: tunable degradation and enhanced mineralization. Composites Science and Technology 147, 8–15.

Zhao, D., Witte, F., Lu, F., Wang, J., Li, J., Qin, L., 2017b. Current status on clinical applications of magnesium-based orthopaedic implants: A review from clinical translational perspective. Biomaterials 112, 287–302.